Supplemental Material: Collective Dynamics and Conformal Ordering in Electrophoretically Driven Nematic Colloids

Arthur V. Straube[1,2,3],* Josep M. Pagès[4],* Pietro Tierno[3,5,6],† Jordi Ignés-Mullol[4,5],‡ and Francesc Sagués[4,5]
[1] *Department of Mathematics and Computer Science, Freie Universität Berlin, Berlin, Germany*
[2] *Group "Dynamics of Complex Materials", Zuse Institute Berlin, Berlin, Germany*
[3] *Departament de Física de la Matèria Condensada, Universitat de Barcelona, Barcelona, Spain*
[4] *Departament de Materiales y Química Física, Universitat de Barcelona, Barcelona, Spain*
[5] *Institut de Nanociència i Nanotecnologia, IN^{2}UB, Universitat de Barcelona, Barcelona, Spain*
[6] *Universitat de Barcelona Institute of Complex Systems (UBICS), Universitat de Barcelona, Barcelona, Spain*

I. MINIMAL MODEL OF PEAR-SHAPED COLLOIDS IN A NEMATIC LIQUID CRYSTAL

In this supplemental material we provide details of a simple model that describes the two-dimensional (in-plane) behavior of weakly asymmetric colloidal particles in a nematic liquid crystal (NLC) confined to a cell, Fig. 1(a). The liquid crystal has a negative dielectric anisotropy leading to the alignement of the director field $\hat{\boldsymbol{n}}(\boldsymbol{r})$ perpendicular to the external alternating (AC) electric field $\boldsymbol{E}(t)$ and parallel to the electrodes. We show that our weakly asymmetric hydrodynamically coupled particles with in-plane positions $\boldsymbol{r}_i = (x_i, y_i)$ effectively approximated by spheres, see Fig. 1(b), are governed by the equation,

$$\frac{d\boldsymbol{r}_i}{dt} = v_0(\omega)\hat{\boldsymbol{n}}(\boldsymbol{r}_i) - \frac{1}{\gamma}\sum_{j\neq i}\frac{\partial U}{\partial \boldsymbol{r}_i}. \tag{1}$$

Here, $v_0(\omega)$ is the frequency-dependent propulsion strength of individual particles along the director $\hat{\boldsymbol{n}}$, U is an interparticle interaction potential, and γ is the friction coefficient. The in-plane director field is taken in the form of the aster pattern, $\hat{\boldsymbol{n}}(\boldsymbol{r}) = -\hat{\boldsymbol{r}}$ [1].

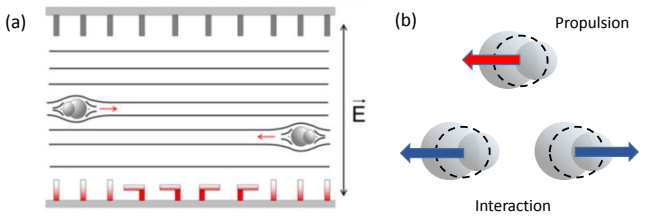

FIG. 1. (a) Schematic showing the experimental cell, with pear-shaped colloids propelled in the nematic liquid crystal with negative dielectric anisotropy under an AC electric field normal to the sample. (b) The hydrodynamic flows around particles lead net propulsion (typically in the direction of the large particle, red arrow, upper panel) caused by the asymmetry of particles and to effective pairwise in-plane pepulsive interactions (blue arrows, lower panel). The weak asymmetry of particles allows us to model them as spheres shown by dashed lines.

In Sec. II we establish an effective repulsion interaction potential stemming from electroosmotic flows generated around particles, which allows us to introduce hydrodynamic coupling between the particles [2, 3]. The same flows together with the asymmetry of particles lead to individual propulsion of particles, as discussed in Sec. III. Further details of interparticle interactions are summarized in Sec. IV. In Sec. V, we provide simple arguments to explain the density profile in a cluster of particles.

II. HYDRODYNAMIC SINGULARITY PERSPECTIVE OF IN-PLANE REPULSION

Here, based on a close analogy with induced charge electroosmosis (ICEO) in isotropic solvents and using hydrodynamic singularity perspective, we outline in-plane long-range hydrodynamic flows, later cast into an effective repulsive potential.

Induced charge electroosmosis. Application of an electric field $\boldsymbol{E} = E_0\hat{\boldsymbol{z}}$ to an unbounded isotropic solvent with an uncharged spherical particle of radius a immersed in it causes an electroosmotic flow around the particle with the velocity field $\boldsymbol{V} = (V_r, V_\theta, V_\varphi = 0)$ of the quadrupolar structure [4, 5], see also Fig. 2,

$$V_r(r,\theta) = \frac{9}{8}V_0\frac{a^2(a^2-r^2)}{r^4}(3\cos^2\theta - 1), \tag{2}$$

$$V_\theta(r,\theta) = \frac{9}{8}V_0\frac{a^4}{r^4}\sin 2\theta, \tag{3}$$

where V_0 is the strength of the flow discussed in Sec. III. This solution can be cast into a scalar streamfunction of the form $\Psi_{\rm ICEO}(r,\theta) = (9/8)V_0a^2(a^2/r^2-1)\sin^2\theta\cos\theta$, with $V_r = (r^2\sin\theta)^{-1}\partial_\theta\Psi$ and $V_\theta = -(r\sin\theta)^{-1}\partial_r\Psi$, which particularly implies the fulfillment of the incompressibility condition, $\nabla\cdot\boldsymbol{V} = 0$.

The far field ($r \gg a$) of this solution, $\boldsymbol{V}_{r\gg a}(r,\theta) = -(9/8)V_0(a/r)^2(3\cos^2\theta - 1)\hat{\boldsymbol{r}} + \mathcal{O}(a^4/r^4)$, which corresponds to the streamfunction,

$$\Psi^{r\gg a}_{\rm ICEO}(r,\theta) = -\frac{9}{8}V_0a^2\sin^2\theta\cos\theta, \tag{4}$$

* Both authors equally contributed to this work
† ptierno@ub.edu
‡ jignes@ub.edu

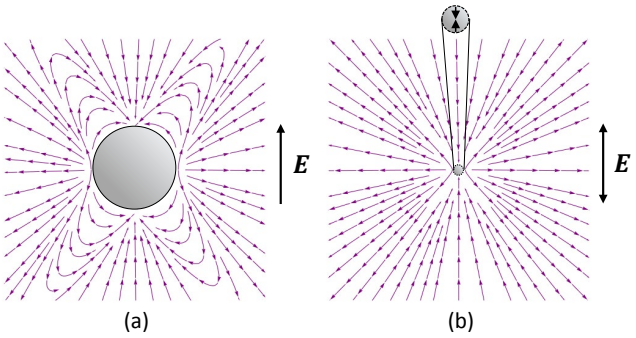

FIG. 2. (a) Quadrupolar electroosmotic velocity flow field $\boldsymbol{V}(\boldsymbol{r})$ generated by an extrenal electric field $\boldsymbol{E}$ around a particle of radius a, as given by Eqs. (2) and (3). (b) The far field $\boldsymbol{V}_{r\gg a}(\boldsymbol{r}) \propto \boldsymbol{S}$ of the flow in (a) is equivalent to the stresslet, cf. Eq. (5) with $\boldsymbol{E} \,||\, \boldsymbol{\nu}$, corresponding to the puller, $\alpha = -1$, see also Fig. 3(b); note the symmetry $\boldsymbol{E} \to -\boldsymbol{E}$.

coincides up to a constant prefactor with the stresslet (or Stokes force dipole), a standard hydrodynamic singularity [6, 7],

$$\boldsymbol{S}(\boldsymbol{r},\boldsymbol{\nu}) = \frac{\alpha}{8\pi\eta r^2}\left[3(\boldsymbol{\nu}\cdot\hat{\boldsymbol{r}})^2 - 1\right]\hat{\boldsymbol{r}}. \tag{5}$$

Expression (5) is generally defined for pushers ($\alpha = +1$) and pullers ($\alpha = -1$), see Fig. 3, with the velocity flow field $\boldsymbol{V}(\boldsymbol{r},\boldsymbol{\nu}) = fl\boldsymbol{S}(\boldsymbol{r},\boldsymbol{\nu})$. Formally, $f \to \infty$, $l \to 0$, whereas their product fl is kept constant.

Because the ICEO flow, Eq. (2), streams towards the particle along $\boldsymbol{E}$ (note that $\boldsymbol{E} \,||\, \boldsymbol{\nu}$ with $\boldsymbol{\nu} = \hat{\boldsymbol{z}}$ and $\boldsymbol{\nu}\cdot\hat{\boldsymbol{r}} = \cos\theta$) at the poles ($V_r < 0$ at $\theta = 0,\, \pi$), and outwards in the equatorial plane ($V_r > 0$ at $\theta = \pi/2$), its flow pattern corresponds to the puller, cf. Figs. 2 and 3. Note the invariance with respect to the change of polarity, $\boldsymbol{\nu} \to -\boldsymbol{\nu}$ (or $\boldsymbol{E} \to -\boldsymbol{E}$), meaning that the flow pattern and streaming direction is preserved also for AC fields.

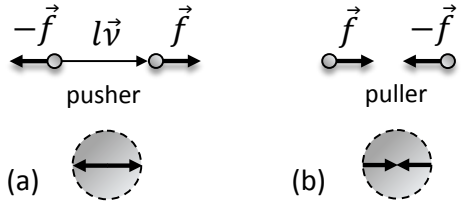

FIG. 3. Construction of the pusher (a) and puller (b) stresslets built of two point forces of opposite signs, $\pm f$, separated by a distance l. The unit vector $\boldsymbol{\nu}$ denotes the direction connecting the two point forces. The forces point either away from (pusher) or towards (puller) each other with their schematic designations below. The flow field around the puller relative to the forces is shown in Fig. 2(b).

Liquid crystal enabled electroosmosis. The case of pear shaped particles in a liquid crystal medium is adapted within two steps.

First, the hydrodynamic field of an asymmetric particle build of a larger and a smaller sphere with slighty different radii, $a_{\rm L} = a + \Delta a$ and $a_{\rm s} = a - \Delta a$, respectively, such that $\Delta a \ll a$, does not substantially differ from that of a spherical particle of radius a at large distances, $r \gg a$. Therefore, we can approximate the long-range hydrodynamic interaction between pear-shaped particles by considering the far fields of effectively spherical particles with a radius $a = (a_{\rm L} + a_{\rm s})/2$.

Second, details on the radial and angular dependence of the velocity field $\boldsymbol{V}(\boldsymbol{r})$ around such a particle can be drawn from recent experiments for spherical particles in an isotropic liquid [8] and a liquid crystal [9] confined to a cell similar to ours, cf. Fig. 1 of the main text. These generic findings together with the symmetry of our system suggest that the leading contribution to the far field for the NLC with the negative dielectric anisotropy and planar anchoring at the particle's surface behaves as $(V_r, V_\theta) \sim -(\cos 2\theta, \sin 2\theta)/r^3$. Thus, although similarly to Eqs. (2) and (3) the flow pattern is quadrupolar with the flow directions corresponding to the puller with respect to $\boldsymbol{E}$ (see Fig. 2), the long-range velocities scale differently with the distance. Accordingly, the hydrodynamic singularity given by Eq. (4), has to be modified, as can be captured in terms of the streamfunction,

$$\Psi_{\rm LC}^{r\gg a}(r,\theta) \propto -V_0\frac{a^3}{r}\sin^2\theta\cos\theta, \tag{6}$$

which satisfies not only the required spatial dependence but also the experimentally confirmed incompressibility of the velocity field at $r \gg a$ [8, 9]. Being interested in the behavior in the plane ("2D") $\theta = \pi/2$ only, similarly to Eq. (5) we have the isotropic in-plane far field,

$$\boldsymbol{V}_{\rm 2D}(a,\boldsymbol{r}) = V_0\frac{a^3}{r^3}\hat{\boldsymbol{r}}, \tag{7}$$

which we can cast into an effective in-plane repulsive potential, see Eq. (12).

III. ELECTROPHORETIC PROPULSION OF INDIVIDUAL PARTICLES

Here we discuss the issue of electrophoretic propulsion of an individual particle and outline the dependence on frequency of its propulsion strength.

For a given slip velocity $\boldsymbol{u}_s$ at the particle's surface, the propulsion velocity of a particle can be rigorously evaluated as an integral, $\boldsymbol{v}_0 = -(4\pi)^{-1}\int \boldsymbol{u}_s {\rm d}\Omega$, where ${\rm d}\Omega$ is an element of the solid angle. Because of perfect symmetry, the slip velocity of a spherical particle, $\boldsymbol{u}_s(\theta) = V_\theta(a,\theta)\hat{\boldsymbol{\theta}}$ with V_θ given by Eq. (3), evidences no net propulsion, $\boldsymbol{v}_0 \equiv 0$. For an asymmetric particle, the perfect symmetry is broken, and the particle starts to propel, $\boldsymbol{v}_0 \neq 0$.

This rigorous approach is, however, no longer helpful for our case because the velocity field in the vicinity of pear-shaped particle in the liquid crystal is unknown. Therefore, we resort to an approximate reasoning capable of capturing the basic physics of propulsion.

Direction of propulsion. In the NLC matrix, the particle alignes its longest axis along the director field as illustrated in Fig. 1. This longitudinal orientation is also preferable for the propulsion because of smaller friction compared to the transverse orientation. The remaining question is whether the particle propels with the small or large lobule ahead.

If we build the pear-shaped particle by combining two stresslets of slightly different strengths, then the net motion would be with the small lobule ahead, Fig. 4(a). Indeed, the motion of a large ("L") and small ("s") particles of radii a_L and a_s coupled by the hydrodynamic field (7) obeys the equations of motion $\dot{\boldsymbol{r}}_\mathrm{L} = \boldsymbol{V}_\mathrm{2D}(a_\mathrm{s}, \boldsymbol{r}_\mathrm{L} - \boldsymbol{r}_\mathrm{s})$ and $\dot{\boldsymbol{r}}_\mathrm{s} = \boldsymbol{V}_\mathrm{2D}(a_\mathrm{L}, \boldsymbol{r}_\mathrm{s} - \boldsymbol{r}_\mathrm{L})$. Let $\boldsymbol{\nu}$ point from the small to large particle and $\boldsymbol{r}_\mathrm{L} - \boldsymbol{r}_\mathrm{s} = l\boldsymbol{\nu}$. By applying the constraint of fixed length on the distance l between the particles and proceeding to the equation for the center of mass, $\boldsymbol{r} = (a_\mathrm{L}\boldsymbol{r}_\mathrm{L} + a_\mathrm{s}\boldsymbol{r}_\mathrm{s})/(a_\mathrm{L} + a_\mathrm{s})$ [2], we find that the propulsion velocity of such a dimer $\dot{\boldsymbol{r}} \propto -(a_\mathrm{L}^3 - a_\mathrm{s}^3)\boldsymbol{\nu}$, i.e. it propels with its small lobule ahead. Here, we have taken into account that the typical ICEO velocity scales linearly with the particle size, $V_0 \propto a$ [5]. As expected, the net motion exists only if the particles are not identical, $a_\mathrm{L} \neq a_\mathrm{s}$. Note, however, that this picture bases entirely on the far fields and is therefore too rough.

A more realistic analysis requires account of the near field. Although its radial dependence is unknown, the normal component of the solvent velocity turns to zero at the particle's surface [9], cf. Eq. (3), which is enough to draw the general conclusion. Let us put, for simplicity, two effective spheres (which differ from the point-like stresslet by accounting for the near field) at a distance $l = a_\mathrm{L}$, see Fig. 4(b). This means that $\boldsymbol{V}_\mathrm{2D}(a_\mathrm{L}, \boldsymbol{r}_\mathrm{s} - \boldsymbol{r}_\mathrm{L})$ has to be set to zero in the above equations of motion and hence $\dot{\boldsymbol{r}}_\mathrm{s} = 0$. As a result, the center of mass velocity $\dot{\boldsymbol{r}} \propto \boldsymbol{\nu}$, and we conclude that such a pear-shaped particle propels with the large lobule ahead, as typically happens in the experiments [10].

Frequency dependent electrophoretic speed. Application of a constant electric field $\boldsymbol{E} = E_0\hat{\boldsymbol{z}}$ causes the formation of an induced-charge screening cloud around the particle. This electric double layer forms within a time τ_s and is characterized by the Debye screening length λ_D and the zeta potential, ζ (the electrostatic potential drop over the screening cloud). The external field sets the electrically charged fluid in the cloud into motion, resulting in the quadrupolar electroosmotic flow. Its intensity and hence the strength of propulsion are determined by the characteristic velocity scale $V_0 = \varepsilon\zeta E/\eta$ [4, 5], cf. Eqs. (2) and (3), with ε and η the dielectric permittivity and viscosity of the solvent, respectively.

For pear-shaped particles, the perfect symmetry of quadrupolar vortices is broken, resulting in a nonzero net propulsion. The frequency dependence of propulsion speed v_0 under AC electric field can be estimated as

$$v_0(\omega) \propto \frac{\varepsilon}{\eta}\overline{\zeta(t)E(t)} = \frac{\varepsilon}{2\eta}\mathrm{Re}[\tilde{\zeta}^*(\omega)\tilde{E}(\omega)], \qquad (8)$$

where overline denotes the time averaging over a period of oscillation, $\zeta(t)$ is taken for a spherical particle, $\tilde{\zeta}(\omega)$ and $\tilde{E}(\omega)$ are complex amplitudes of $\zeta(t)$ and $E(t)$ introduced as $F(t) = \mathrm{Re}[\tilde{F}(\omega)\mathrm{e}^{\mathrm{i}\omega t}] = [\tilde{F}(\omega)\mathrm{e}^{\mathrm{i}\omega t} + \tilde{F}^*(\omega)\mathrm{e}^{-\mathrm{i}\omega t}]/2$ with the superscript "$*$" for complex conjugation.

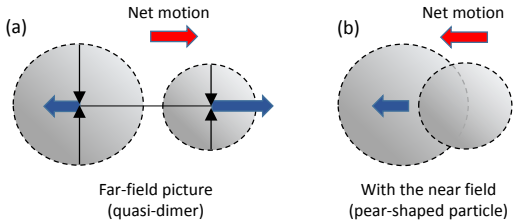

FIG. 4. (a) Quasi-dimer built of a pair of stresslets of different strengths. (b) A more realistic picture accounting for the near field that provides the direction of propulsion consistent to the experiment. Here, the center of the smaller particle locates exactly at the surface of the larger particle.

In contrast to the unbounded system, in the cell geometry the upper and lower confining planes are electrodes separated by a distance L, Fig. 1. Similarly to the particle, electric double layers are formed around the electrodes, which screen the external field prescribed at the electrodes as $\boldsymbol{E}_\mathrm{e}(t) = E_\mathrm{e}(t)\hat{\boldsymbol{z}}$, $E_\mathrm{e}(t) = E_0\cos\omega t$ within the timescale $\tau_\mathrm{e} = \lambda_\mathrm{D}L/(2D)$, with D the solvent diffusivity. The electric field in the bulk obeys a relaxation equation $\dot{E}(t) = -\tau_\mathrm{e}^{-1}E(t) + \dot{E}_\mathrm{e}(t)$, yielding

$$\tilde{E}(\omega) = \frac{\mathrm{i}\omega\tau_\mathrm{e}}{1 + \mathrm{i}\omega\tau_\mathrm{e}}E_0. \qquad (9)$$

The electric field in the bulk is screened at low frequencies, $E \ll E_0$ for $\omega\tau_\mathrm{e} \ll 1$, and persists at high frequencies, $E \approx E_0$ for $\omega\tau_\mathrm{e} \gg 1$, when the double layer has no time to develop near the electrodes.

Further, for the zeta potential we have up to the angular dependence [4],

$$\tilde{\zeta}(\omega) \propto \frac{1}{1 + \mathrm{i}\omega\tau_\mathrm{s}}\tilde{E}(\omega)a, \qquad (10)$$

where the charging time of a spherical particle $\tau_\mathrm{s} = \lambda_\mathrm{D}a/(2D)$. Evaluating Eq. (8) with expressions (9) and (10), we arrive at the estimate for the self-propulsion speed of individual particle, $v_0(\omega) \propto (\varepsilon E_0^2 a/\eta)\tau_\mathrm{e}^2\omega^2(1 + \tau_\mathrm{s}^2\omega^2)^{-1}(1 + \tau_\mathrm{e}^2\omega^2)^{-1}$, represented as

$$v_0(\omega) = u_0\alpha(\omega), \quad \alpha(\omega) = \frac{(\tau_\mathrm{s} + \tau_\mathrm{e})^2\omega^2}{(1 + \tau_\mathrm{s}^2\omega^2)(1 + \tau_\mathrm{e}^2\omega^2)}. \qquad (11)$$

Here, dimensionless frequency function $\alpha(\omega) \in [0, 1]$ and the prefactor $u_0 \propto (\varepsilon E_0^2 a/\eta)\tau_\mathrm{e}^2/(\tau_\mathrm{s} + \tau_\mathrm{e})^2$ has the units

of velocity. The constant u_0 is determined by fitting this dependence against experimental data, see the main text and Fig. 1(e) there. A similar approach was successfully used to justify the propulsion of spherical inclusions with hedgehog defects in a NLC [11]. Although formula (11) is formally similar to that obtained earlier [11], the definitons of the timescale τ_s differ, which is a consequence of using different theories: the two-dimensonal theory for a cylinder [5] in Ref. 11 and for a sphere [4, 5] here.

Equation (11) remains formally valid under following conditions. First, the time-averaging approach utilized in Eq. (8) tacitly assumes that the electric double layer changes quasi-steadily [5], which requires that frequencies are not too high, $\omega \ll \omega_D = \tau_D^{-1}$, where $\tau_D = \lambda_D^2/D$ is the electrolyte relaxation time. Second, our analysis is based on the assumptions of thin electric double layers and small particles, $\lambda_D \ll a \ll L$, which automatically entails the separation of timescales, $\tau_D \ll \tau_s \ll \tau_e$. Third, the external fields are supposed to be not too strong [4].

IV. PAIRWISE INTERACTION POTENTIAL

Hydrodynamically induced repulsion. Because the mechanisms of hydrodynamically induced repulsion and individual propulsion considered in Secs. II and III originate from the same osmotic flows, their frequency dependence is the same. Furthermore, we cast the far field velocity distribution, Eq. (7), into the effective hydrodynamically induced repulsive potential,

$$U_{hd}(r,\omega) = A\frac{\alpha(\omega)}{r^2}, \tag{12}$$

with the frequency dependence in $\alpha(\omega)$ given by Eq. (11).

Induced electrostatic dipolar repulsion. As argued in the main text, there should be an additional electrostatic-based repulsion mechanism, with a different frequency dependence. In our experiments, polarizable particles are coplanar, and the dipoles induced by the electric field are perpendicular to the plane of the sample. This results in a net pairwise repulsion (see Fig. 3(b) in the main text) that we introduce in the model with the potential $U_{dd}(r) \propto \boldsymbol{p}^2/r^3$.

Induced dipole moments $\boldsymbol{p}$ appear as a result of charge separation leading to the formation of electric double layers surrounding each particle. While flows originated in the double layers lead to the hydrodynamic interaction among particles, their polarization makes them interact electrostatically. In an AC electric field, $\boldsymbol{E}(t) = \mathrm{Re}[\tilde{E}(\omega)e^{i\omega t}]\hat{\boldsymbol{z}}$, the induced dipole moment of a particle can be written as [4, 5]

$$\boldsymbol{p} \propto \mathrm{Re}\left[\left(\frac{1/2 - i\omega\tau_s}{1 + i\omega\tau_s}\right)\tilde{E}(\omega)e^{i\omega t}\right]\hat{\boldsymbol{z}}\,,$$

valid under the same conditions as for self-propulsion, Sec. III. Taking into account the expression for the field in the bulk, Eq. (9), and averaging over time, we obtain

$$U_{dd}(r,\omega) = B\frac{\beta(\omega)}{r^3}, \quad \beta(\omega) = \frac{(1/4 + \tau_s^2\omega^2)\tau_e^2\omega^2}{(1+\tau_s^2\omega^2)(1+\tau_e^2\omega^2)},$$

with the frequency-independent prefactor B.

Short-range repulsion. The finite particle size is accounted by the steep short-range repulsive potential

$$U_{hc}(r) = 4\epsilon\left[\left(\frac{\sigma}{r}\right)^{48} - \left(\frac{\sigma}{r}\right)^{24} + \frac{1}{4}\right],$$

which is applied at distances $r < 2^{1/24}\sigma$ and is otherwise zero. We set the strength of short-range interactions such that $4\epsilon/\gamma = 1\,\mu\mathrm{m}^2/\mathrm{s}$, and choose the effective diameter $\sigma = 4.3\,\mu\mathrm{m}$ of the particles to be slightly of their real size to reflect the experimentally observed fact that particles in a cluster do not come into contact. Local defects or thin boundary layer-like vortex flows attached to the surface of the particles [9, 12] are potential reasons why the particles cannot approach each other beyond the certain distance.

Elastic liquid crystal interactions. We also account for the interactions mediated by the elasticity of the liqiud crystal matrix, which are responsible for the optimal particle arrangement, described by

$$U_{qq}(\boldsymbol{r},\hat{\boldsymbol{n}}) = \frac{C}{r^5}(3 - 30\cos^2\vartheta + 35\cos^4\vartheta),$$

with $\vartheta = \vartheta(\boldsymbol{r},\hat{\boldsymbol{n}})$ the angle between the vector connecting the centers of particles, $\boldsymbol{r}$, and the far-field orientation of the nematic director, see Fig. 3(c) in the main text.

V. ONE-DIMENSIONAL MODEL OF A CLUSTER OF DRIVEN REPELLING COLLOIDS

Here we propose a simplified one-dimensional model of a cluster of phoretic particles that admits an approximate analytic expression for their density in the cluster as a function of radial distance from its center.

Consider a number N of particles with radial coordinates r_i $(i = 1, ..., N)$ that propel with the phoretic speed v_0 against the center of the cluster, $r = 0$, with an immobile particle placed at $r_0 = 0$. Assuming a finite size of particles as ensured by a short-range repulsive potential, the equilibrium configuration corresponds to equidistant spacing of particles with $r_i = iq$, where q is an equilibrium effective "hard-core" distance.

Assuming that the particles are additionally subject to long-range repulsive interactions according to a potential $U(r)$, as e.g. in Eqs. (1) and (12), which alter the equidistant particle spacing,

$$\Delta r_i := r_i - r_{i-1} = q + \Delta q_i, \quad \Delta q_i \geq 0. \tag{13}$$

To make analytical progress, we assume nearest-neighbor interaction and a harmonic approximation for the repulsive potential, $U(q + \Delta q_i) \approx U(q) + U'(q)\Delta q_i +$

$U''(q)\Delta q_i^2/2$, with $\Delta q_i \ll q$. Here, the prime denotes the derivative of potential. As a result, the equilibrium configuration of particles obeys the set of equations

$$\gamma v_0 = -U''(q)\Delta q_i + U''(q)\Delta q_{i+1}, \quad i = 1, \ldots, N-1$$
$$\gamma v_0 = -U'(q) - U''(q)\Delta q_N, \quad i = N.$$

By taking the sum of equations i to N, finding $\Delta q_i = Q - (N - i + 1)\ell$ and substituting it into Eq. (13), for interparticle distances we obtain

$$\Delta r_i = q + Q - (N - i + 1)\ell, \tag{14}$$

where $Q = -U'(q)/U''(q) \geq 0$ and $\ell = \gamma v_0/U''(q) \geq 0$. Considering relation (14) recursively for different i, we find for the coordinates, $r_i = iq + iQ - i\left[N - (i-1)/2\right]\ell$.

To proceed to the continuum limit, we consider $N \gg 1$, put $r := r_i$ and solve the above quadratic equation with respect to i to obtain two solutions $i_\pm(r) = -\ell^{-1}(q + Q - N\ell) \pm \ell^{-1}\sqrt{(q + Q - N\ell)^2 + 2\ell r}$. Note that because by definition $\Delta q_i \geq 0$ for all i, $(q + Q - N\ell) \geq 0$ and the solution $i_-(r)$ is physically unjustified, we proceed further with $i(r) := i_+(r)$.

As follows from Eq. (14) for $N \gg 1$, $\Delta r_i = q + Q - N\ell + i\ell$ and with account of $i(r)$, for the one-dimensional number density $\rho(r)$ defined as $1/\Delta r_i$ we obtain

$$\rho(r) = \frac{1}{\sqrt{(q + Q - N\ell)^2 + 2\ell r}} = \frac{\rho_*}{\sqrt{1 + 2\rho_*^2 \ell r}}. \tag{15}$$

Here, $\rho_* = (q + Q - N\ell)^{-1}$ is a maximum number density, as follows from the above equation at $r = 0$, which corresponds to the shortest interparticle distance, $\Delta r_1 = (q + Q - N\ell)$. We finally note that our smallness assumption, $\Delta q_i \ll q$, implies that solution (15) is justified for small enough $\ell \simeq O(q/N)$ and can be expanded. Therefore, the number density decays linearly with r,

$$\rho(r) \approx \rho_* - \frac{\rho_*^3 \gamma v_0}{U''(q)} r, \tag{16}$$

with the negative slope $d\rho/dr \propto -\gamma v_0/U''(q)$, which is proportional to the strength of propulsion and inversely proportional to the repulsion strength.

[1] A. V. Straube, J. M. Pagès, A. Ortiz-Ambriz, P. Tierno, J. Ignés-Mullol, and F. Sagués, New J. Phys., **20**, 075006 (2018).

[2] A. Baskaran and M. C. Marchetti, Proc. Nat. Acad. Sci. USA, **106**, 15567 (2009).

[3] D. L. Piet, A. V. Straube, A. Snezhko, and I. S. Aranson, Phys. Rev. Lett., **110**, 198001 (2013).

[4] V. A. Murtsovkin, Colloid Journal, **58**, 358 (1996).

[5] T. M. Squires and M. Z. Bazant, Journal of Fluid Mechanics, **509**, 217 (2004).

[6] O. S. Pak and E. Lauga, in *Fluid-Structure Interactions in Low-Reynolds-Number Flows*, edited by C. Duprat and H. A. Stone (The Royal Society of Chemistry, 2016) Chap. 4, pp. 100–167.

[7] M. Lisicki and G. Nägele, in *Soft Matter at Aqueous Interfaces. Lecture Notes in Physics*, Vol. 917, edited by P. Lang and Y. Liu (Springer, 2016) Chap. 10, pp. 313–386.

[8] C. Peng, I. Lazo, S. V. Shiyanovskii, and O. D. Lavrentovich, Phys Rev E, **90**, 051002 (2014).

[9] I. Lazo, C. Peng, J. Xiang, S. V. Shiyanovskii, and O. D. Lavrentovich, Nat Commun, **5**, 5033 (2014).

[10] S. Hernàndez-Navarro, P. Tierno, J. Ignés-Mullol, and F. Sagués, Mol. Cryst. Liq. Cryst., **610**, 163172 (2015).

[11] O. D. Lavrentovich, I. Lazo, and O. P. Pishnyak, Nature, **467**, 947 (2010).

[12] C. Conklin, O. M. Tovkach, J. Viñals, M. C. Calderer, D. Golovaty, O. D. Lavrentovich, and N. J. Walkington, Phys. Rev. E, **98**, 022703 (2018).